

Microstructural evaluation of fatigue damage in SA533-B1 and type 316L stainless steels

C. Y. CHEN

Institute of Nuclear Energy Research (INER), Lungtan, Taiwan, ROC
E-mail: cychen@iner.gov.tw

J. Y. HUANG

Institute of Nuclear Energy Research (INER), Lungtan, Taiwan, ROC;
Department of Mechanical Engineering, National Central University, Taiwan, ROC

J. J. YEH, R. C. KUO

Institute of Nuclear Energy Research (INER), Lungtan, Taiwan, ROC

J. R. HWANG

Department of Mechanical Engineering, National Central University, Taiwan, ROC

J. G. HUANG

Nuclear Operation Department, Taiwan Power Company, Taipei, Taiwan, ROC

Transmission electron microscopy (TEM) examinations were made on fatigued SA533-B1 low alloy steel and Type 316L stainless steel specimens with the intention to investigate the mis-orientation changes among dislocation cells and the evolution of dislocation structures. Contrary to what might be expected for the cell structures, no clear relationship between fatigue damage and the mis-orientation changes of cell walls (or subgrain boundaries) was found in the fatigued samples of SA533-B1 steel (a bcc structure); however, significant changes of dislocation structures were observed in the fatigued samples of Type 316L stainless steel (an fcc structure). This could be accounted for by their different structures as well as complicated defect structures such as subgrain boundaries, small carbides, and dislocations inhomogeneously distributed in the SA533-B1 steel. It is interesting to note that at room temperature dislocations of fatigued SS316L specimens were observed to arrange themselves on {111} slip planes, in contrast, at 300°C the dislocations tend to move from their slip planes into subgrain boundaries in the surface layers rather than in the cross sectional layers. © 2003 Kluwer Academic Publishers

1. Introduction

Fatigue damage has been recognized as one of the most important failure causes in many structural components. Since the fatigue damage is structure sensitive, it is important to understand the microstructural changes in materials of different crystal structures during fatigue deformation. Several transmission electron microscopy (TEM) investigations of the fatigued samples by Fukuoka and Nakagawa [1–3] have shown that the mis-orientation of dislocation cells increased as a function of the fatigue life of a low alloy steel SA508. If this is the case, the accumulation of fatigue damage could be related to mis-orientation changes of dislocation cell (i.e., subgrain) structures. However, no similar effect has been reported on another low alloy steel SA533-B1 with similar chemical composition, or other types of material system. The present work was thus attempted to investigate whether dislocation cell-to-cell mis-orientation (θ) is appreciably changed in fatigue-damaged specimens using the SA533-B1 steel (a body-centered cubic structure) as a model material which is

widely used for constructing commercial reactor pressure vessels. Efforts were also made to examine the arrangement of dislocations in a less complicated material Type 316L stainless steel (a face-centered cubic structure). It will be of interest to compare the microstructure of a bcc material with that of an fcc one for a better understanding of microstructural evolution with fatigue damage.

2. Mis-orientation analysis

In order to accurately measure the mis-orientation between adjacent dislocation cells in fatigued samples, the method adopted in this study was not quite the same as that used by Fukuoka *et al.* [2]. In their methods, the selected area diffraction patterns (SADPs) taken from five different areas in each grain were exposed on the same film. The maximum angular deviation on the negative, where the five diffraction patterns were superimposed, was measured and regarded as one datum. In general, there could be three sources of error in the

TABLE I Chemical compositions of SA533-B1 and Type 316L stainless steels (wt %)

Materials	Elements										
	C	Si	Mn	P	S	Ni	Mo	Cr	Al	Cu	Fe
SA533-B1 ^a	0.207	0.22	1.28	<0.02	0.006	0.61	0.52	N/A ^b	0.015	0.03	Bal.
Type 316L	0.02	0.3	1.46	0.03	<0.02	12.3	0.53	17.1	N/A ^b	N/A ^b	Bal.

^aSolution treated at 900°C for one hour, then quenched and tempered at 670°C for one hour.

^bN/A = Not available.

mis-orientation results measured by Fukuoka *et al.* The first source of error is the deviation caused by each of five slightly different zones (or projections) on one negative for the corresponding areas in each grain. In our study, we have found this source of error can be up to 5°. This deviation can be corrected using a double-tilt goniometer stage and tilting the diffraction patterns to the same simple zone axis such as [111]. Instead of one-dimensional measurement of the angular deviation as described by Fukuoka *et al.*, the mis-orientation θ can be more accurately calculated with a three-dimensional formula of $\sqrt{\theta_x^2 + \theta_y^2 + \theta_z^2}$, where θ_x was determined as an angular deviation between SADPs superimposed on the same film, θ_y and θ_z were another two angular deviations obtained by tilting adjacent dislocation cells (i.e., subgrains) to the same zone axis. The second source of error is due to the unavoidable bending of the TEM thin foil. Since the mis-orientation between SADPs would increase with increasing distance between the positions of the selector apertures, one should not attempt to select many different areas covering few cell structures as described in Fukuoka's papers, but should put the position of the selector aperture on each side of a selected cell wall, and then from these two SADPs, the mis-orientation between adjacent cells can be more accurately measured. The bending error in current study can be reduced to be <0.5° with a diameter of $\sim 5 \mu\text{m}$ selected for SADP, while the errors from the Fukuoka's results could be several degrees depending on the distance between the selector aperture positions and variation of bending on the thin foil. The third source of error involves inhomogeneous microstructure; i.e., the measured areas in the thin foil are not representative of the fatigued sample.

Another approach for determining the orientation relationship between grains is to use Kikuchi-diffraction patterns as commonly adopted by the microscopist. However, this method has limitations of its own, for example, a distinguishable Kikuchi-diffraction pattern is taken from a specific thickness of the specimen which will limit the measured areas. Furthermore, it may need many computer simulations to successfully match TEM patterns for more accurate mis-orientation measurement. For engineering purposes, it is impractical and too time-consuming to use this approach for the mis-orientation analysis. For a low-angle grain boundary with $\theta < 10^\circ$, as is the case in this study, it should be sufficient to calculate the mis-orientation θ between subgrains with a three-dimensional formula of $\sqrt{\theta_x^2 + \theta_y^2 + \theta_z^2}$.

3. Experimental

The materials under investigations were commercial Type 316L stainless steels, and SA533-B1 reactor pressure vessel (RPV) steels which were manufactured by the China Steel Corporation in accordance with ASTM Specification A533-93 [4]. Their chemical compositions and mechanical properties are listed in Tables I and II, respectively.

The high-cycle fatigue specimens of a plate type with a gauge length of 30 mm were prepared and tested according to the ASTM Specification E466. Fig. 1 shows the dimensions of the test specimen. Before testing, all the specimens have been well polished as per the recommendations of ASTM E466. Fatigue tests were performed with a 100 KN MTS 810 close-loop servohydraulic machine under load control with a sinusoidal wave form or under strain control with a triangular wave; stress ratios ($\sigma_{\min}/\sigma_{\max}$) or strain ratios ($\varepsilon_{\min}/\varepsilon_{\max}$) were set at 0.2 or -1 at room temperature or 300°C. The steel specimens were loaded in the rolling direction. The test conditions and results are summarized in Table III. A digital video camera and an *in situ* optical microscope with a magnification of 20× were used to monitor crack initiation.

TABLE II Mechanical properties of SA533-B1 and Type 316L stainless steels

Materials	Properties			
	UTS ^a (MPa)	YS ^b (MPa)	TE ^c (%)	UE ^d (%)
SA533-B1	722	650	29.5	10.2
Type 316L	530	236	68	54

Tested data presented in this table are the averaged values of duplicated tests.

^aUTS = Ultimate tensile strength.

^bYS = Yield strength.

^cTE = Total elongation.

^dUE = Uniform elongation.

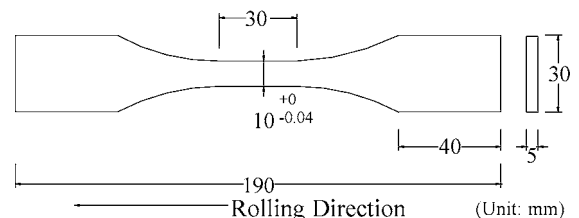


Figure 1 Dimensions of a fatigue specimen.

TABLE III Fatigue test conditions and results of SA533-B1 and Type 316L stainless steels

Materials	Conditions				
	Test temperature (°C)	Total stress range ($\Delta\sigma_f$) or strain range ($\Delta\varepsilon_f$)	Stress ratio ($\sigma_{\min}/\sigma_{\max}$) or strain ratio ($\varepsilon_{\min}/\varepsilon_{\max}$)	Frequency (Hz)	Number of cycles to failure (N)
SA533-B1	RT ^a	546 MPa	0.2	20	292,143
	RT ^a	1.4%	-1	0.14	3,429
Type 316 L	RT ^a	392 MPa	-1	5	74,444
	300	318.6 MPa	-1	20	28,704

^aRT = Room temperature.

To examine fatigue effects on the evolution of dislocation structures and to compare the surface microstructure with that of the bulk of fatigue-tested specimens, TEM samples, with surface layers and cross sectional layers normal to the loading axis, were prepared from as-received and fatigued specimens. In order to prevent the final plastic deformation from complicating the fatigue structure, the sampling position should be kept away from the necking region, but as close to the final fracture site as possible. TEM samples were polished with fine emery paper to a thickness of 0.1 mm, then chemically thinned with a double-jet polishing machine in a solution of 10 vol% perchloric acid (HClO₄) and 90 vol% methanol (CH₃OH) at ~10 V and -30°C. TEM examination was performed on a JEM-2000FX electron microscope operated at 200 kV, equipped with a GATAN model 646-M double-tilt analytical holder (two orthogonal tilt axes) for measuring tilt angles of the specimen.

4. Results and discussion

4.1. SA533-B1 RPV steel

As analyzed in the previous section, the mis-orientation θ between adjacent cells (i.e., subgrains) should be measured by applying the three-dimensional formula of $\sqrt{\theta_x^2 + \theta_y^2 + \theta_z^2}$. The significant contributions of two angular deviations (θ_y and θ_z) to mis-orientation were confirmed by the demonstration experiments here, as shown in Fig. 2. Firstly, the grain A is tilted so that its beam direction is very close to [111] zone axis (which can be recognized by the uniform intensity of spots in the diffraction pattern [5]), while grain B close to [111] zone axis, as seen from the inset diffraction patterns in Fig. 2a. Secondly, the values of θ_y and θ_z between adjacent cells were then obtained by tilting grain B to the orientation very close to [111] zone axis, as seen in Fig. 2b. Finally, the angular deviation θ_x was measured from the superimposed diffraction patterns of grain A and grain B, as seen in Fig. 2c. The results indicated that θ_x was measured to be about 0.4°, while $\sqrt{\theta_y^2 + \theta_z^2}$ was about 5°. Apparently, lack of consideration for the contributions of θ_y and θ_z (due to slightly deviated zone axis between adjacent cells) can result in a significant amount of error while measuring mis-orientation θ . It is thus clear that the mis-orientation in subgrains should not be represented only by one angular deviation θ_x obtained from superimposed diffraction patterns.

Fig. 3 shows the TEM images with microstructures typical of surface layers and cross sectional layers

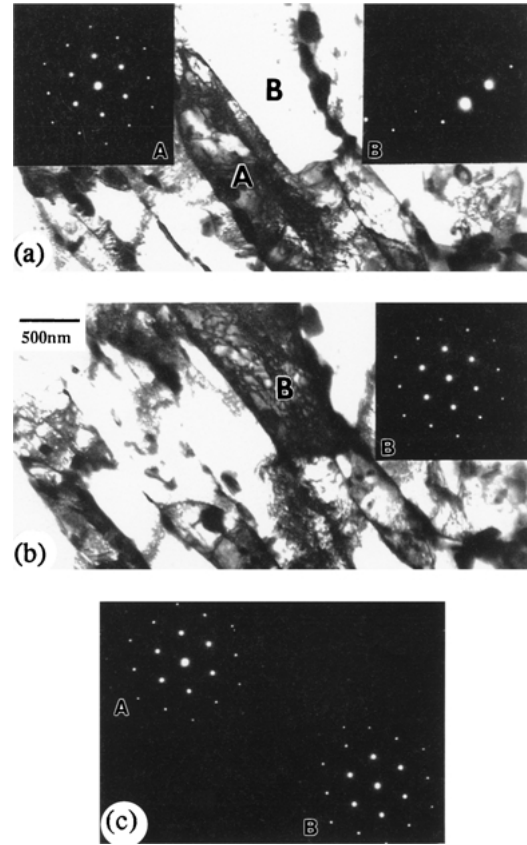


Figure 2 Demonstration experiments showing the procedures of measuring three angular deviations (θ_y , θ_z and θ_x): (a) TEM bright-field image with inset diffraction patterns showing grain A very close to [111] zone axis, while grain B close to [111] zone axis. (b) TEM bright-field image after tilting grain B through θ_y and θ_z to the beam direction very close to [111] zone axis. θ_y and θ_z were measured as 5° and 0.2°, respectively. (c) Superimposed diffraction patterns (very close to [111] zone axis) from grain A and grain B for measuring θ_x . θ_x was measured as 0.4°. Scale bar in (a) apply to (b) as well.

from as-received and fatigued SA533-B1 specimens. These specimens were characterized by the complicated defect structures such as subgrain boundaries, small carbides, and dislocations. The characteristic of the subgrain structure was found to be prevalent in the as-received and the fatigued specimens. However, no appreciable changes was observed not only between surface layers and cross sectional layers but also between extremely different fatigue-tested conditions (such as high-cycle and low-cycle fatigue tests), as can be seen in Fig. 3. The mis-orientation θ between adjacent cells was also calculated with a three-dimensional formula of $\sqrt{\theta_x^2 + \theta_y^2 + \theta_z^2}$, as described above. It was found that the mis-orientation θ randomly distributed

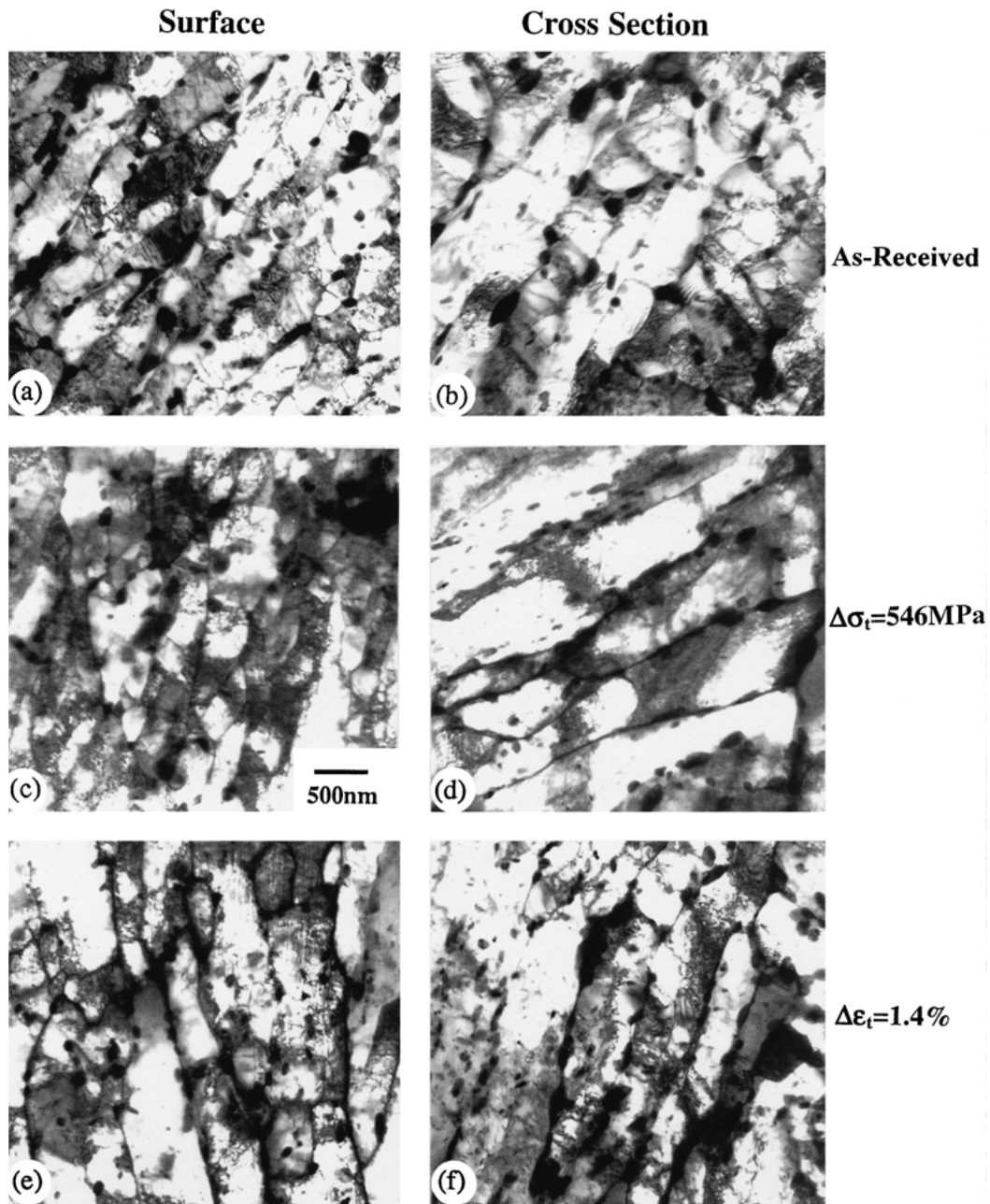


Figure 3 TEM images of SA533-B1 showing no appreciable changes of subgrain structures in (a,b) as-received specimens, (c,d) high-cycle fatigued specimens with $\Delta\sigma_t = 546$ MPa, and (e,f) low-cycle fatigued specimens with $\Delta\varepsilon_t = 1.4\%$. Scale bar in (c) apply to all images as well.

from 1° to 5° and no tendency toward a specific value based on more than ten measurements. The results in this work indicated that no discernible changes of microstructures can be identified with the TEM images of fatigued samples owing to the complicated and inhomogeneously distributed defect structures in this kind of alloy steel.

4.2. Type 316L stainless steel

Although the accumulation of fatigue damage related to the mis-orientation changes of dislocation cell structures has not been discovered in a bcc structure such as SA533-B1, an attempt was made on a material with the fcc structure. We exemplify here the importance of making such observations on Type 316L stainless steel. Fig. 4 shows the TEM images with typical microstructures of surface layers and cross sectional layers from

as-received and fatigued specimens of Type 316L stainless steels. As can be seen in the as-received materials (see Fig. 4a and b) the microstructure of surface layers was different from that of the cross sectional layers, which was caused by surface work-hardening on the plates during rolling as the dislocation density in surface structure is much higher than that of the bulk structure. In the cross sectional layers, planar defects (see Fig. 4b) exhibiting fringe contrast are generally described as stacking faults or microtwins due to their similar contrast. Microtwins, which are closely structurally related to stacking faults, has been fully discussed by Chen and Stobbs [6]. Such thin twins are observed to be distorted and associated with dislocations after fatigue tests, as shown in Fig. 4d and f. It is noteworthy that in the surface layers of fatigue-tested specimens at room temperature, dislocations were observed to arrange themselves on $\{111\}$ slip planes, as illustrated in

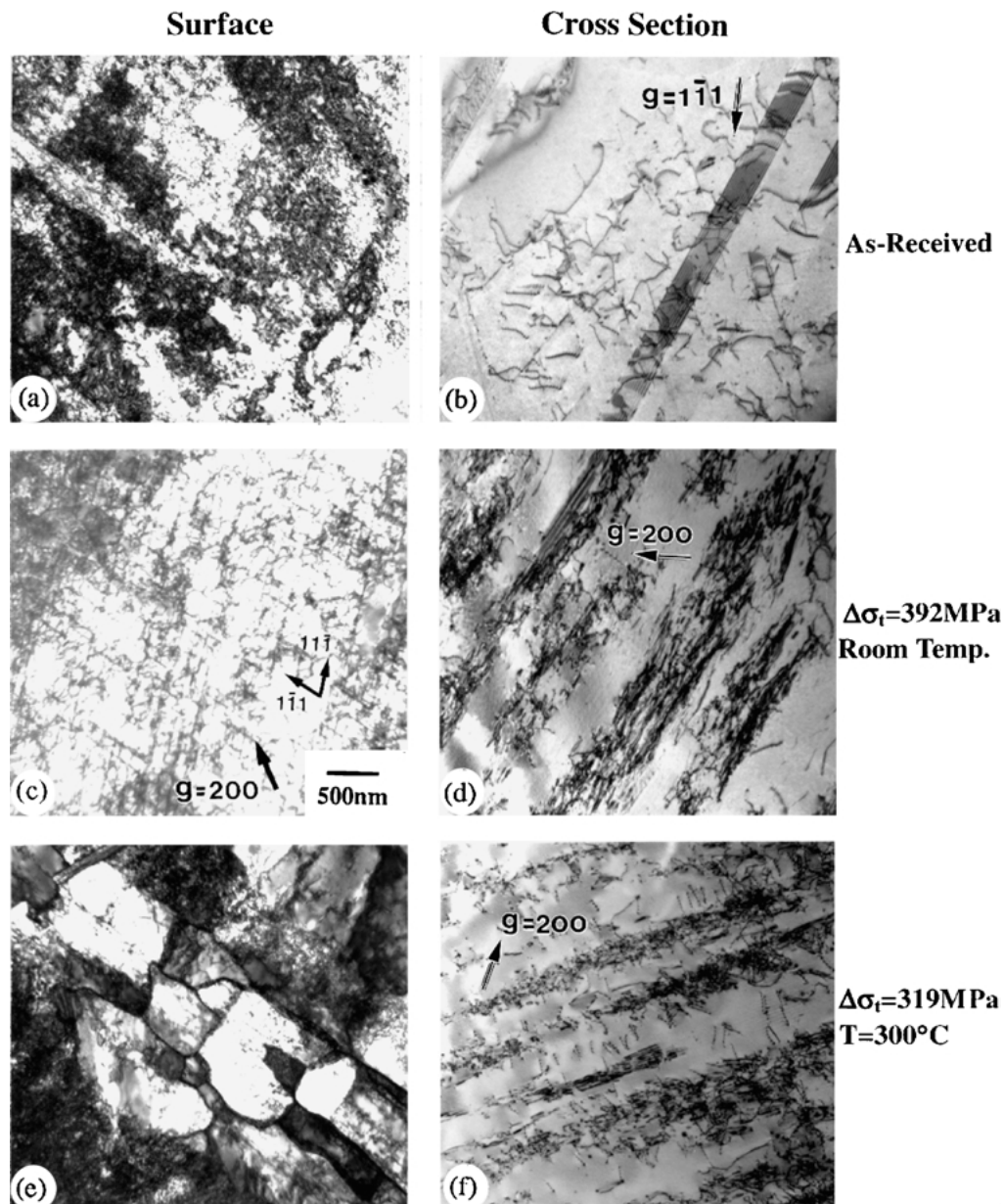


Figure 4 TEM images of Type 316L showing significant changes of microstructures between surface layers (a,c,e) and cross sectional layers (b,d,f). (a,b) as-received specimens, (c,d) fatigued specimens tested with $\Delta\sigma_t = 392$ MPa at room temperature, and (e,f) fatigued specimens tested with $\Delta\sigma_t = 319$ MPa at $T = 300^\circ\text{C}$. Micrographs were taken with the beam direction near to [011]. Scale bar in (c) apply to all images as well.

Fig. 4c, while at a temperature of 300°C the dynamic recovery occurred, as illustrated in Fig. 4e. This is because the movement of the dislocations (resulting from plastic deformation by surface hard working) from their slip planes into subgrain boundaries (or cell walls) lowers the average strain energy associated with the dislocations [7] and thus tends to lower the effective rate of work-hardening produced by the fatigue test. These subgrain boundaries are clearly demonstrated by the inset diffraction patterns in Fig. 5 showing low-angle boundaries (i.e., the subgrain boundaries are demonstrated by the inset diffraction patterns in each grain which is near to [011] zone under the same imaging condition). The dynamic recovery in Type 316L stainless steel is believed to be connected with the test temperature and dislocation density. The effects of temperature and surface dislocations (both remained in as-received specimens and produced by fatigue tests) on the dynamic recovery need to be clarified by further

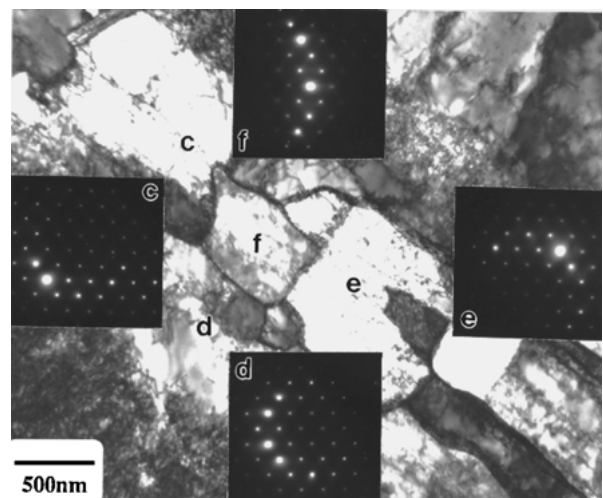


Figure 5 TEM image in Fig. 4e showing subgrain boundaries as illustrated by the inset diffraction patterns in each subgrain which is near to [011] zone under the same imaging condition.

experiments and observations. In this study, however, we have found that the failure mechanism of the fatigue for the Type 316L stainless steel at 300°C might be influenced by the dynamic recovery if the dislocation density in surface layers is sufficiently high as is often the case with commercial alloys.

5. Conclusions

It has been demonstrated that the mis-orientation θ between adjacent subgrains can be measured by applying the three-dimensional formula of $\sqrt{\theta_x^2 + \theta_y^2 + \theta_z^2}$, instead of θ_x only, since the contributions of another two angular deviations (θ_y and θ_z) to mis-orientation cannot be ignored, as shown by TEM investigations in this study. It should be noted that either no tendency of mis-orientation changes between adjacent cells or no discernible changes of microstructures were observed with the fatigued samples of SA533-B1 steel (a bcc structure); however, significant changes of dislocation structures were observed with the fatigued samples of Type 316L stainless steel (an fcc structure). A comparison of a bcc and an fcc structure showed that the fatigue damage is structure sensitive; besides, complicated and inhomogeneous defect structures (such as subgrain boundaries, small carbides, and dislocations) were found to be a primary factor that made the quantitative, even qualitative, tasks of the TEM results more difficult in SA533-B1 than in Type 316L. It is worth emphasizing that no correlation between the fatigue damage and the mis-orientation changes of subgrain structures has been observed in the present study, whereas

the movement of dislocations into subgrain boundaries (i.e., the dynamic recovery) has been noted for the first time in the fatigued samples of Type 316L stainless steel. Since the dynamic recovery was found to occur at 300°C in the surface structure rather than in the bulk structure, it is suggested that the effects of the surface structure and temperature on the fatigue damage have to be considered cautiously in the evaluation of the fatigue failure mechanism.

Acknowledgment

The authors are grateful for the financial support of the Taiwan Power Company, Taiwan, ROC.

References

1. C. FUKUOKA and Y. G. NAKAGAWA, *Scripta Mater.* **34** (1996) 1497.
2. C. FUKUOKA, H. YOSHIKAWA, Y. G. NAKAGAWA and M. E. LAPIDES, *Metall. Trans. A* **24A** (1993) 2209.
3. Y. G. NAKAGAWA, H. YOSHIKAWA and M. E. LAPIDES, *ibid.* **21A** (1990) 1989.
4. ASTM A533/A533M-93, "Standard Specification for Pressure Vessel Plates, Alloy Steel, Quenched and Tempered, Manganese-Molybdenum and Manganese-Molybdenum-Nickel."
5. J. W. EDINGTON, "Practical Electron Microscopy in Material Science" (Macmillan, London, 1976) p. 56.
6. C. Y. CHEN and W. M. STOBBS, *Ultramicroscopy* **58** (1995) 289.
7. R. E. REED-HILL, "Physical Metallurgy Principles" (Van Nostrand Company, New York, 1973) p. 282.

Received 6 November 2001

and accepted 17 October 2002